Journal of Science and Sustainable Development (JSSD), 2026, 14(2), 14-30

ISSN: 2304-2702 (print); 2414-4479 (online)
DOI: 10.20372/au.jssd.14.2.2026.0750

RESEARCH PAPER

Historical and Future Land Use and Land Cover Dynamics in the Erer Sub-Basin Wabi-Shebelle River Basin, Ethiopia

Birhanu Legesse Wakjiraa[1*], Asfaw Kebede Kassa[2], Awdenegest Moges[3], and Olkeba Tolessa Leta[4]

[1]*Ph.D. candidate, Department of Natural Resources Management, Ambo University, Ethiopia. +251 0920901147, birelegesse2000@gmail.com, https://orcid.org/0009-0008-7237-4315*

[2]*Hydraulics and Water Resource Engineering, Haramaya Institute of Technology, Ethiopia. asfaw649@gmail.com, https://orcid.org/0000-0002-6496-7216*

[3]*Department of Agricultural Engineering, Hawassa University, Ethiopia. awde_moges@yahoo.co.uk https://orcid.org/0000-0001-6084-8327.*

[4]*St. Johns River Water Management District, Palatka, FL, United States. olkebat2005@gmail.com, https://orcid.org/0000-0003-3479-901X*

** The corresponding author: birelegesse2000@gmail.com*

Abstract

Rapid land use and land cover (LULC) change threatens ecosystem sustainability, yet its future patterns and dynamics remain insufficiently understood in developing countries like Ethiopia. The study aimed to evaluate the historical LULC changes and predict its future changes in the northeast of the Wabi-Shebelle River Basin (WSRB), Ethiopia. We used the Support Vector Machine (SVM) algorithms in ArcGIS Pro to classify LULC classes from multi-sensor Landsat imagery (MSS, ETM+, OLI). The Cellular Automata (CA)-Markov model and Land Change Modeler (LCM) in TerrSet with Idrisi software were used to predict future LULC changes. Between 1985 and 2022, water bodies, forests, and shrub lands decreased by 84.1%, 47.4%, and 22.6%, respectively, whereas built-up, agricultural, and barren lands increased by 2862.4%, 44.6%, and 75.5%, respectively. By 2062, under the business-as-usual scenario, water bodies, forests, and shrub lands are projected to decline by 80.1%, 40.1%, and 19.8%, respectively, while developed, agricultural, and barren lands are expected to increase by 566.3%, 18.5%, and 4.9%, respectively. The SVM and CA–Markov models effectively classified historical LULC and simulated future changes. Although LULC conversion is projected to continue, its rate is expected to slow as much of the highly suitable land, particularly in the upper region, has already been converted. Sustainable land management and targeted conservation measures should be prioritized to limit further LULC conversion and protect the remaining natural ecosystems, particularly in the upper region.

Keywords: LULC; SVM; CA-Markov; Wabi-Shebelle River Basin

Introduction

Land use and land cover (LULC) dynamics refer to the spatial and temporal changes in land use (the management and utilization of land for specific purposes) and land cover (the physical and biological features covering the Earth's surface) (Cumani and Latham, 2015; Kutter *et al*., 2016). These changes are driven by both natural processes and human activities, resulting in continuous landscape transformation over time (Demissie *et al*., 2017; Horamo *et al*., 2021). The LULC transformations have profound impacts on ecosystem services (Zhao *et al*., 2020), biodiversity (Yohannes *et al*., 2017), hydrological processes (Balha *et al*., 2023), soil quality (Bekele, 2019), climate regulation, and socioeconomic development (Roy *et al*., 2022). Sustainable land management, environmental preservation, and well-informed decision-making all depend on an understanding of these shifts.

Advances in satellite remote sensing have made it possible to obtain accurate and consistent Earth observation data, while GIS enables the storage, integration, analysis, and visualization of spatial data, enabling detection of historical LULC changes. Landsat imagery is one of the most popular remotely captured datasets for LULC mapping due to its free accessibility, moderate spatial resolution, and long-term archive (Goward *et al*., 2006). These satellite data can be analyzed, categorized, and combined with supplementary geographical data in a GIS system to produce trustworthy LULC maps.

Several techniques for classifying satellite images have been developed for LULC mapping, including supervised methods such as Maximum Likelihood Classification (MLC), Minimum Distance, Decision Tree (DT), Random Forest (RF), Artificial Neural Networks (ANN), and Support Vector Machine (SVM), as well as unsupervised approaches such as ISODATA and K-means clustering (Debnath *et al*., 2023). Among these methods, SVM has become well-known because of its capacity to handle non-linear class boundaries and spectrally comparable land cover types while reliably classifying multispectral satellite imagery with few training samples (Saigal, 2021). Compared with other machine learning algorithms such as artificial neural networks (ANN) and deep learning models, SVM requires fewer training samples, lower computational resources, and less parameter tuning while maintaining competitive classification accuracy over a larger area (Jozdani *et al*., 2019). Because of these benefits, SVM is a suitable and reliable classifier for creating precise historical LULC datasets from Landsat imagery.

Similarly, numerous future LULC dynamics simulation models have been developed, including Markov Chain (Bell, 1974), Cellular Automata (CA) (White and Engelen, 1993), CA-Markov (Eastman, 2020), CLUE-S (Conversion of Land Use and its Effects at Small Regional Extent) (Verburg *et al*., 2002), Artificial Neural Network (ANN)-based models (Pijanowski *et al*., 2002), and the more recent Patch-generating Land Use Simulation (PLUS) model (Liang *et al*., 2021). Even though these models have proven to be highly predictive, many of them need large datasets relating to socioeconomics, the environment, and policy, as well as complex calibration techniques and a lot of processing power. Each model differs in how it reflects temporal transitions, allots space, and integrates environmental and socioeconomic driving forces.

In this study, we employed a CA–Markov model, which provides a practical balance between model simplicity, spatial realism, and prediction accuracy by combining the strengths of Markov chain analysis and CA. Markov chains model class transitions, and cellular automata spatially allocate them via neighborhood rules (Eastman, 2020). The Kappa indices of agreements are used to statistically evaluate the agreement between the simulated and actual LULC maps, a crucial process in LULC map prediction (van Vliet *et al*., 2011).

In Ethiopia, especially in the northeastern region of the WSRB, where high population density, persistent food insecurity (Assede *et al*., 2023), and climate changes (Toni et al., 2022) put growing pressure on land resources, rapid LULC change is a significant environmental challenge for sustainable development. Although LULC dynamics have been investigated in some watersheds within the basin (Hailu, 2024), the northeast WSRB remains poorly studied, and its future LULC trajectories have not been assessed, which limits evidence-based land management and sustainable planning in the region.

This study aims to (i) assess the historical LULC dynamics of the northeast WSRB using SVM-based classification and (ii) predict future LULC changes by integrating the CA–Markov model, thereby providing insights to support sustainable land-use planning and resource management.

Materials and Methods

Study Area

This study was carried out in one of the biggest sub-basins in the northeast WSRB. It is situated geographically between latitudes 7° 33′ N and 9° 30′ N and longitudes 41° 37′ E and 42° 26′ E with elevation ranging from 481 to 3383 m above sea level. The study area has three major watersheds, namely Gobele, Erer, and Erer-guda (Fig. 1).

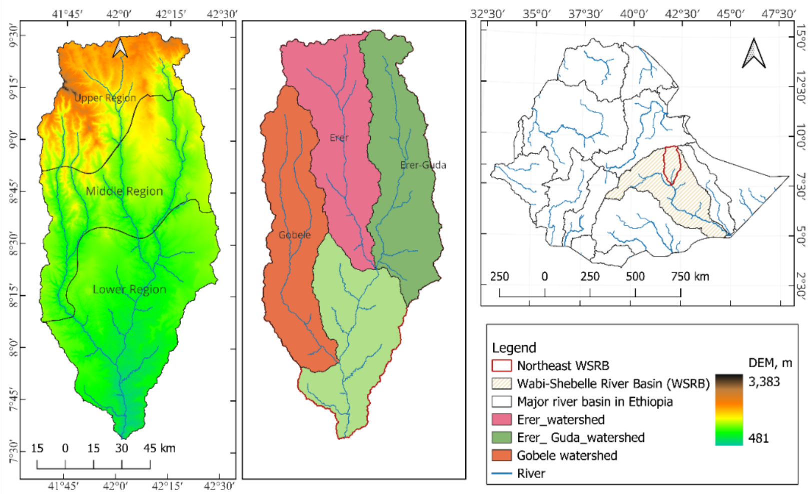

Figure 1. Location and geographical characteristics of the northeast Wabi-Shebelle River Basin: the subdivision of the sub-basin (upper, middle, and lower regions); the Digital Elevation Model (DEM); and the major watersheds (Erer, Erer-Guda, and Gobele watersheds).

In order to account for the variations in surface reflectance of satellite images, the study area was divided into three regions—upper (24.32%), middle (33.62%), and lower (42.06%)—based on the agro-ecology (Table 1). In the upper region, the ranges of annual precipitation and temperature are 600–1,260 mm and 16–28°C, respectively. The lower region receives annual precipitation ranging between 250 and 500 mm and a mean temperature between 20 and 35°C.

Table 1. Upper, middle, and lower regions of the study area based on agroecology.

Regions	Agro-ecological zones	Area (Km^2)
Upper	Tepid to cool sub-moist mid-highlands (SM2) Tepid to cool moist mid-highlands (M2) Tepid to cool sub-humid mid-highlands (SH2) Tepid to cool humid mid-highlands (H2)	3605.61 (24.32%)
Model	Hot to warm sub-moist lowlands (SM1) Hot to warm, moist lowlands (M1) Hot to warm subhumid lowlands (SH1)	4984.63 (33.62%)
Lower	Hot to warm arid lowland plains (A1). Hot to warm semi-arid lowlands (SA1)	6236.28 (42.06%)

Source: Ministry of Water and Energy of Ethiopia.

The hot lowland area is lightly populated and practices a pastoral farming system, herding drought-resistant livestock, mainly camels, goats, sheep, and cattle. On the other hand, the upper region is heavily populated and uses a mixed agricultural system with intensive, integrated crop-livestock mixed farming systems with key crops like khat, sorghum, maize, potatoes, and other vegetables.

From field observation, the major LULC includes agricultural land, shrub land, barren land, waterbodies, forests, and built-up areas. In the upper region of the study area, due to the small average landholding size, less than 0.85, of households, they opt for farming cash crops (khat, coffee) and cattle fattening (Tadesse *et al*., 2014). There is hardly any communal grassland, and the main sources of cattle feed are crop wastes and the leaves of fodder bushes and trees (Tadesse *et al*., 2014). Thus, grassland and swampy areas are not considered in the LULC classification because they cover insignificant areas of land.

The major geological formation is sedimentary formations, with Precambrian rocks and metamorphic rocks outcropping (Kebede, 2015NWRC, 1973). The dominant soil types include Calcaric regosols, Eutric nitisols, Eutric regosols, Dystric cambisols, and Humic cambisols. The available hydrological data is sparse, with most stations not properly installed, resulting in low flow series with zero value (Awass, 2009).

Image Acquisition, Pre-processing, and Classification

Landsat imagery (Table 2) for 1985, 2000, and 2022 was acquired from the U.S. Geological Survey (USGS) Earth Explorer (https://glovis.usgs.gov). Landsat images were chosen due to their accessibility and long-term availability (Zhang et al., 2022). The images from December to February were selected for their cloud-free and similar vegetation status.

Table 2. Landsat images and their characteristics. Where MSS (Multispectral Scanner), ETM+ (Enhanced Thematic Mapper Plus), OLI (Operational Land Imager), and TIRS (the Thermal Infrared Sensor).

Product	Sensor	Acquisition Date (yyyy/mm/dd)	Path/Row	Resolution (m)	Day/night
Landsat 3	MSS	1985/01/20 1985/01/20	166/54,55	30	Day
Landsat 7	ETM+	2000/12/23 2000/12/07	166/54,55	30	Day
Landsat 8	OLI/TIRS	2022/01/26	166/54,55	30	Day

Source*:* (https://glovis.usgs.gov**)**

Images were subjected to pre-processing to execute radiometric and atmospheric rectifications and to augment the quality of Landsat imagery utilizing the Semi-Automatic Classification Plugin (SCP) of QGIS (Congedo, 2021). Ground control points were used to conduct geometric correction, which eradicates geometric distortions present in satellite imagery.

The LULC classifications were performed using a Support Vector Machine (SVM) model in ArcGIS Pro. The study employed a supervised object-based classification method with a minimum of two segments, considering the spatial resolution of Landsat imagery and the study area's size. The SVM was selected because it has a record of accomplishment of achieving a higher level of overall classification accuracy than the other machine learning algorithms (Basheer *et al*., 2022; Woldemariam *et al*., 2022).

Table 3. LULC descriptions

LULC class	Description
Water (Wa)	Surface water bodies like rivers, lakes, wetlands, and ponds.
Barren (Ba)	Bare lands, sediment deposits at the bank of rivers, degraded hill land, construction areas, and rocky areas.
Agriculture (Ag)	Land designated for the cultivation of crops, intercropping (crops + khat), and irrigated area.
Developed (De)	Residential, commercial areas, industrial establishments, roads, and other uncategorized surface pavements.
Shrub (Sh)	Areas covered with shrubs, bushes, and acacia mixed with herbs and grasses.
Forest (Fo)	Areas covered with either dense natural trees, plantations, or parks.

Source: Author.

Post-processing

Accuracy assessment

We collected 678 ground reference points using a global positioning system (GPS) for 2022, while the reference points created in ArcGIS Pro were obtained from a Google Earth Pro image with an acquisition date like the Landsat imagery for 1985 and 2000. A stratified random sampling method was employed to ensure enough samples across all LULC classes (FAO, 2016). We estimated the number of reference points (N) using Equation (1) (Olofsson *et al.*, 2014).

$$N = \left(\frac{\sum W_i * S_i}{SE}\right)^2$$

Where SE is the standard error of estimated overall accuracy (OA) that we would like to achieve, W_i is the mapped proportion of the area of class i, and S_i is the standard deviation of stratum i.

The overall accuracy (OA) was calculated from the error matrix to assess the classification accuracy across the LULC classes (Congalton and Green, 2019; FAO, 2016). Cohen's Kappa coefficient (K), which is a vigorous nonparametric statistical measure, was employed to consider the land use classification by chance (Rwanga and Ndambuki, 2017). The value of K ranges from -1 to 1, where a kappa of -1, 0, and 1 indicate disagreement, agreement by chance, and perfect agreement, respectively (Viera and Garrett, 2005) (Table 4).

Table 4. Over all accuracy (OA), Producer's accuracy (PA), user's accuracy (UA), and Kappa coefficient (K) of Land use/Land cover (LULC) classification for a) 1985, b) 2000, and c) 2022. Google Earth Pro Image was used as references in the 1985 and 2000, whereas, ground reference points (collected using GPS) were used for reference in 2022.

a)	Reference from Google Earth Pro, 1985								
	LULCC	Wa	De	Fo	Ba	Sh	Ag	Total	UA
Classified Landsat image (10 and 11 February, 1985)	Wa	72	0	3	0	0	1	76	0.95
	De	0	80	0	4	0	1	85	0.94
	Fo	7	0	79	1	6	2	95	0.83
	Ba	1	2	0	76	3	6	88	0.86
	Sh	1	2	12	11	202	4	232	0.87
	Ag	1	0	4	3	6	123	137	0.90
	Total	82	84	98	95	217	137	713	713
	PA	0.88	0.95	0.81	0.8	0.93	0.9		
Kappa coefficient = 0.86 and Overall accuracy = 0.89									
b)	Reference from Google Earth Pro, 2000								
	LULCC	Wa	De	Fo	Ba	Sh	Ag	Total	UA

Classified Landsat image (date:07 and 23 December 2000)	Wa	64	0	1	3	0	1	69	0.93
	De	1	80	0	12	1	1	95	0.84
	Fo	2	0	98	0	0	3	103	0.95
	Ba	1	2	2	121	8	7	141	0.86
	Sh	0	0	1	2	120	4	127	0.94
	Ag	2	2	0	0	6	107	117	0.91
	Total	70	84	102	138	135	123	652	652
	PA	0.91	0.95	0.96	0.88	0.89	0.87		
	Kappa coefficient = 0.88 and Overall accuracy = 0.90								
c)	Reference from Ground Truth, collected using GPS								
	LULC	Wa	De	Fo	Ba	Sh	Ag	Total	UA
Classified Landsat image (date:26 February 2022)	Wa	76	0	3	1	3	1	84	0.9
	De	0	80	1	8	1	6	96	0.83
	Fo	2	0	90	1	6	1	100	0.90
	Ba	0	2	0	109	4	2	117	0.93
	Sh	2	0	6	7	144	2	161	0.89
	Ag	0	0	0	4	12	104	120	0.87
	Total	80	82	100	130	170	116	678	
	PA	0.95	0.98	0.90	0.84	0.85	0.90		
	Kappa coefficient = 0.87 and Overall accuracy = 0.89								

LULC change analysis

The annual rates (r) of change for different LULC classes were determined by employing the formula based on compound interest law as suggested by Puyravaud (2003) (Equation 2). The comprehensive dynamic degree (c) of LULC gives the degree of intensity of LULC change during the study period. It was determined using Equation (3) (Wang *et al.*, 2020).

$$r = \frac{1}{(t_2 - t_1)} \ln\left(\frac{A_2}{A_1}\right) \qquad \textbf{(1)}$$

Where A_1 and A_2 are areas of LULC class at the time t_1 and t_2, respectively.

$$c = \left(\frac{\sum_{i=1}^{n} \Delta S_{i=j}}{2\sum_{i=1}^{n} S_i}\right) / t \, * 100 \qquad \textbf{(2)}$$

where S_i is the area of classified land-use type at the initial time of the study; $\Delta S_{i=j}$ the absolute value of the area in which class i converted to class j in the research period, i ≠ j; n is the number of land-use types in the area, and t is the length of the monitoring period.

LULC Change Prediction and Validation

The AC-Markov model within Land Change Modeler (LCM) in TerrSet was used to predict the LULC of 2042 and 2062. The AC-Markov, which utilizes the transitional probability matrix, was used due to its capability of forecasting the states of LULC based on historical conditions. The CA-Markov model is used most frequently because it integrates the advantages of cellular automata and Markov chain analysis to predict future land use trends based on its change history (Eastman, 2020; Gebresellase *et al*., 2023).

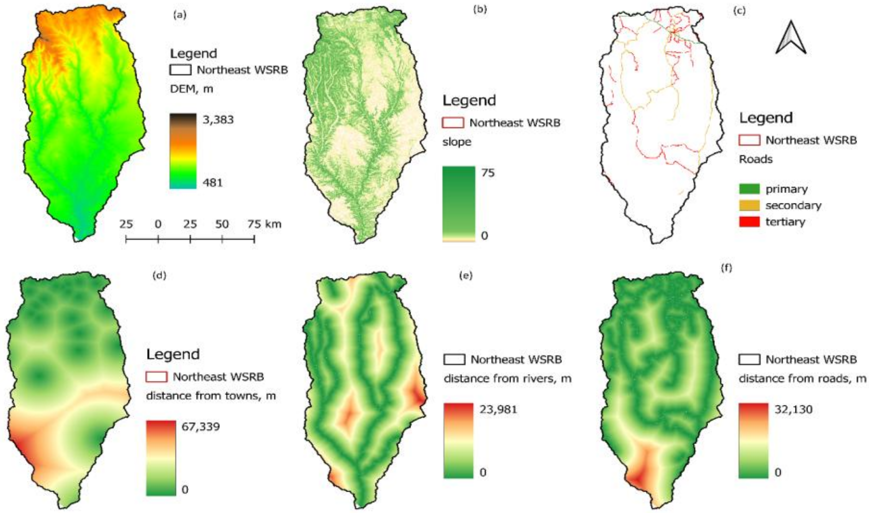

Figure 2. Driving variables for LULC transition in LCM: (a) Digital Elevation Model (DEM), (b) slope in degrees, (c) basic road networks, (d) distance from city center, (e) distance from river, and (f) distance from roads.

Historical LULC maps and spatial driver variables like stream network, land slope, road network, DEM, and city center were utilized for predicting LULC change. A DEM with a spatial resolution of 30 m was obtained from the Advanced Spaceborne Thermal Emission and Reflection Radiometer (ASTER) (https://search.earthdata.nasa.gov/). Road networks were extracted from the Open Street Map (https://www.openstreetmap.org/). The developed areas were extracted from the classified LULC map of 2022. The Euclidean distance method in the ArcGIS Pro platform was used to develop the distance from streams, road networks, and the city center (Fig. 2).

LULC maps of 1985 and 2000 were used to simulate the LULC map of 2022, which was used to evaluate the model's prediction capability. The study used LULC maps from 2000 and 2022 to predict potential transitions between LULC classes, and a transition matrix was estimated to predict future LULC changes for 2042 and 2062.

The Kappa indices of agreement were used to evaluate the agreement between the classified and simulated LULC map in 2022. Kappa indices of agreements—Kappa for location ($K_{location}$), Kappa standard ($K_{standard}$), and Kappa for no information (K_{no})–were employed to compare the classified and the simulated LULC in 2022 (van Vliet *et al*., 2011). Kappa indices of agreement range from 0 to 1. Where Kappa < 0.5 indicates a rare agreement, 0.5 < Kappa < 0.75 indicates a moderate level of agreement, 0.75 < Kappa < 1 indicates a high degree of agreement, and Kappa = 1 indicates complete agreement (Munthali *et al*., 2020).

Results

Historical LULC Maps

Table 5 and Fig. 3 show LULC classes in the upper, middle, and lower regions of the northeast WSRB between 1985 and 2022. For users, producers, overall accuracy, and the Kappa coefficient shown in Appendix Table 1, higher classification accuracies, more than 80%, were achieved.

Table 5. LULC classes (in km² and %), classification overall accuracy, and Kappa coefficient in the Upper, Middle, and Lower regions of NEWSRB for the years 1985, 2000, and 2022.

Year	**ID**	**Upper Region**		**Middle Region**		**Lower Region**		**Total**	
		Area, km²	**%**	**Area, km²**	**%**	**Area, km²**	**%**	**Area, km²**	**%**
1985	Water	17.40	0.48	6.43	0.13	18.53	0.30	42.40	0.29
	Developed	2.60	0.07	1.70	0.03	0.38	0.01	4.70	0.03
	Forest	249.80	6.9	182.20	3.70	195.10	3.20	627.10	4.23
	Barren	225.80	6.3	663.50	13.3	736.80	11.90	1626.10	10.97
	Shrubs	1140.50	31.6	3501.30	70.40	5199.00	83.90	9840.70	66.37
	Agriculture	1969.60	54.6	629.20	12.70	88.00	1.40	2686.70	18.12
Overall Accuracy		0.89		0.87		0.87			
Kappa Coefficient		0.90		0.87		0.84			
2000	Water	9.50	0.26	0.70	0.01	14.09	0.23	24.30	0.16
	Developed	25.00	0.69	6.22	0.12	0.46	0.01	31.60	0.21
	Forest	193.30	5.40	92.30	1.90	314.70	5.50	630.40	4.25
	Barren	398.80	11.10	1033.00	20.70	1473.90	23.20	2875.60	19.39
	Shrubs	949.90	26.40	2909.30	58.40	4289.00	68.80	8148.20	54.95
	Agriculture	2029.10	56.30	942.80	18.90	145.60	2.30	3117.50	21.02
Overall Accuracy		0.92		0.90		0.87			
Kappa Coefficient		0.90		0.87		0.84			
2022	Water	1.00	0.03	0.54	0.01	5.19	0.08	6.80	0.05
	Developed	103.20	2.86	29.00	0.58	5.55	0.09	137.80	0.93
	Forest	109.80	3.00	97.20	2.00	122.80	2.00	329.80	2.22
	Barren	247.50	6.90	1106.60	22.20	1499.40	24.00	2853.50	19.25
	Shrubs	721.00	20.00	2411.00	48.40	4484.00	71.90	7615.90	51.37
	Agriculture	2423.10	67.20	1340.30	26.90	119.30	1.90	3882.80	26.19
Overall Accuracy		0.89		0.89		0.89			
Kappa Coefficient		0.86		0.86		0.85			

The results indicate that agriculture has become the dominant land use in the upper region, covering 54.6% of the area. Moreover, the agricultural coverage has increased from 2686.70 km² (18.12%) in 1985 to 3882.80 km² (26.19%) in 2022 in the entire study area (Fig. 3).

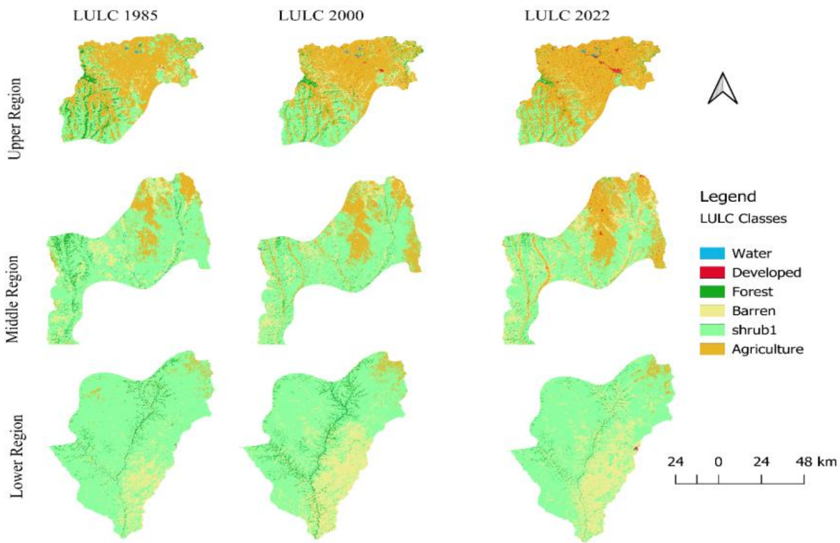

Figure 3. LULC class map during 1985, 2000, and 2022 in the upper, middle, and lower regions of the study area (Note: The map directions, legends, and scales are for all maps).

The developed area has also expanded during the study period, particularly in the upper region. In 1985, the built-up area in the upper region covered less than 0.10% (2.60 km²); by 2022, it accounted for 2.86% (103.20 km²). On the other hand, barren land covered 11.9% of the lower region in 1985 and 1499.40 km² (24%) in 2022.

Change in LULC

Table 6 shows the Northeast WSRB experienced substantial LULC changes between 1985 and 2022. Water bodies, forests, and shrub lands decreased by 84.1%, 47.4%, and 22.6%, respectively, whereas built-up, agricultural, and barren lands increased by 2862.4%, 44.6%, and 75.5%, respectively. These changes indicate intensive conversion of natural land covers to human-dominated land uses, primarily driven by agricultural expansion, urbanization, and land degradation.

Table 6. LULC changed during 1985–2000, 2000–2022, and 1985–2022 (in km² and %).

LULC	Area (Km²)			Change in %		
	1985	2000	2022	2042-2022	2062-2042	2062-2022
Water	42.40	24.30	6.80	-42.70	-72.20	-84.10
Developed	4.70	31.60	137.80	580.30	335.50	2831.90
Forest	627.10	600.40	329.80	-4.30	-45.10	-47.40
Barren	1626.10	2905.60	2853.50	78.70	-1.80	75.50
Shrubs	9840.70	8148.20	7615.90	-17.20	-6.50	-22.60
Agriculture	2686.70	3117.50	3883.80	16.00	24.60	44.60

Additionally, the intensity of land-use change during the study period was analyzed using the comprehensive dynamic degree of land-use classes. The comprehensive dynamic degree of land-use change obtained in the upper, middle, and lower regions from 1985 to 2022 were 0.31%, 0.24%, and 0.10%, respectively. The highest and lowest dynamic degrees of land use were observed in the upper and lower regions, respectively.

Transition Among LULC Classes

Table 7 shows the LULC transition area matrix between 1985–2000 and 2000–2022, in which parts of the classes exchanged to other class and some part was gained from the other classes. For instance, most shrub land was converted to barren land (1,517.1 km²) and agricultural land (969.4 km²), indicating substantial land degradation and agricultural expansion. On the other hand, shrub land gained 315.8 and 381.5 km² from forest and barren land, respectively. Developed land also gained significant area during the study period at the expense of agricultural land (12.2 km^2) and shrub lands (10.2 km^2) which might indicate urbanization has been a major factor in the LULC dynamics due to rapid population growth.

Table 7. Transition area matrix (km^2), gains and losses of LULC classes between 1985 and 2000, and 2000 and 2022.

LULC classes		**2000**							
		Wa	**De**	**Fo**	**Ba**	**Sh**	**Ag**	**Total**	**Loss**
1985	Water (Wa)	**23.80**	0.10	1.80	2.90	1.90	12.00	42.40	18.60
	Developed (De)	0.00	**4.50**	0.10	0.10	0.10	0.00	4.70	0.20
	Forest (Fo)	0.10	0.60	**223.10**	34.30	315.80	53.30	627.20	404.10
	Barren (Ba)	0.10	4.20	35.60	**1103.10**	381.50	101.90	1626.20	523.10
	Shrubs (Sh)	0.10	10.20	315.30	1517.10	**7028.60**	969.40	9840.80	2812.20
	Agriculture (Ag)	0.20	12.20	24.60	248.10	420.40	**1980.90**	2686.30	705.40
Total		24.30	31.70	600.40	2905.60	8148.20	1136.50	14827.50	
Gain		0.50	27.20	377.30	1802.50	1119.60	1136.50		

LULC classes		**2022**							
		Wa	**De**	**Fo**	**Ba**	**Sh**	**Ag**	**Total**	**Loss**
2000	Water	**6.80**	0.00	0.20	4.80	5.00	8.40	24.20	18.40
	Developed	0.00	**30.00**	0.40	0.20	0.60	0.60	31.70	1.70
	Forest	0.10	3.00	**218.50**	11.30	275.80	91.70	600.40	381.90
	Barren	0.10	5.70	2.30	**1737.20**	904.00	256.30	2905.60	1168.40
	Shrubs	0.10	13.30	81.90	934.00	**6257.80**	861.20	8148.20	1890.40
	Agriculture	0.70	85.80	26.60	166.00	172.90	**2665.60**	3117.40	451.80
Total		6.80	137.80	329.80	2853.50	7615.90	3883.80	14827.50	
Gain		0.90	107.80	111.30	1116.30	1358.10	1218.20		

Predicted LULC map for 2042 and 2062

Table 8 reveals that the projected and change in 2022–2062, slower than that of the historical change rate. Water bodies, forests, and shrub lands are projected to decline by 80.1%, 40.1%, and 19.8%, respectively, while built-up, agricultural, and barren lands are expected to increase by 566.3%, 18.5%, and 4.9%, respectively. The lower rates of change relative to the historical period suggest a gradual stabilization as well as the degradation of the landscape.

Table 8. Present and predicted LULC of the northeast WSRB. LULC 2022 is based on Landsat 8 image classification using a Support Vector Machine (SVM).

LULC	**Area (Km^2)**			**Change in %**		
	2022	**2042**	**2062**	**2042-2022**	**2062-2042**	**2062-2022**
Water	6.80	5.31	4.06	-21.90	-23.50	-40.25
Developed	137.80	406.93	918.18	195.31	125.63	566.31
Forest	329.80	228.83	197.44	-30.62	-13.72	-40.13
Barren	2853.50	2898.71	2992.33	1.58	3.23	4.87
Shrubs	7615.90	7079.92	6111.63	-7.04	-13.68	-19.75

Agriculture	3883.80	4208.20	4603.70	8.35	9.40	18.54

The LULC maps for 2042 and 2062 were predicted using the CA-Markov model in Idrisi software after obtaining satisfactory Kappa indices of agreement between actual and predicted LULC maps in 2022. Kappa indices of agreement—$K_{location}$ (0.82), $K_{standard}$ (0.75), and K_{no} (0.80)–were attained in the evaluation of the model's LULC change prediction capability. Fig. 4 illustrates the projected LULC changes from the base year 2022 to 2042 and 2062 (Fig. 4).

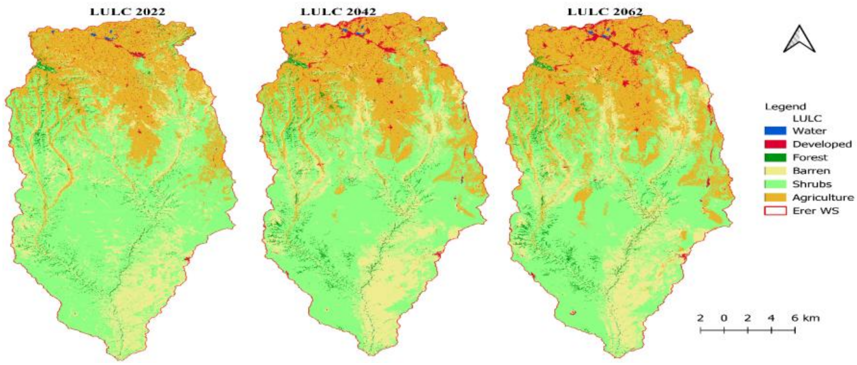

Figure 4. LULC maps in 2022, 2042 and 2062

Discussions

Historical LULC Changes

Figure 4 shows the base LULC map (2022) and predicted LULC maps for 2042 and 2062. The transition probability matrix is given in Table 9. The LULC projection reveals a significant landscape transformation by 2062, dominated by rapid urban expansion, which is projected to increase by 92.8% (2042) and 122.8% (2062) relative to the 2022 baseline. Agricultural land is also projected to slightly expand. This growth in developed and agricultural areas occurs at the direct expense of natural landscapes, with forest, shrub land, and barren land all showing a consistent decline over the projection period.

Table 9. Transition Probability matrix of change between LULC classes in 2042 and 2062

2042						
LULC	Wa	De	Fo	Ba	Sh	Ag
Wa	0.65	0.01	0.02	0.13	0.13	0.06
De	0	0.62	0.01	0.10	0.09	0.19
Fo	0	0.00	0.62	0.03	0.27	0.07
Ba	0	0.01	0.00	0.77	0.15	0.07
Sh	0	0.00	0.01	0.08	0.87	0.05
Ag	0	0.01	0.00	0.03	0.04	0.91
2062						
LULC	Wa	De	Fo	Ba	Sh	Ag
Wa	0.39	0.02	0.03	0.22	0.24	0.11
De	0.00	0.35	0.01	0.16	0.16	0.33
Fo	0.00	0.00	0.35	0.07	0.46	0.12
Ba	0.00	0.01	0.00	0.6	0.26	0.13
Sh	0.00	0.00	0.01	0.13	0.77	0.09
Ag	0.00	0.02	0.01	0.05	0.09	0.83

The results of the analysis of historical LULC dynamics showed substantial changes have been undergone in the northeast WSRB from 1985 to 2022. The region's population growth (ESS, 2023) and urbanization have led to the expansion of built-up areas, while the demand for food has led to an increase in agricultural coverage. The expansion of agricultural land at the expense of forest, on the other hand, could aggravate soil erosion and reduce water resources (Wolde *et al*., 2023; Woldemariam and Harka, 2020), particularly in the upper region. The developed and agricultural land decreases toward the sub-outlet, which might be associated with low population density. On the other hand, the barren and shrub land area increases toward the lower end of the sub-basin, which could be due to climatic changes such as drought and rising temperatures and mismanagement of land resulting in land degradation (Grover and Musick, 1990).

Moreover, the analysis also showed that the area coverage of water bodies, forests, and shrub land continuously declined over the study period. A decrease in water bodies could negatively affect freshwater availability for aquatic ecosystems, agricultural production, and domestic consumption. This finding is consistent with the review of Regasa *et al*. (2021) on LULC analyses in Ethiopia, where natural land has widely transitioned to developed uses, agriculture, and commercial infrastructure. Between 2000 and 2022, developed areas in Africa increased by 68% due to urbanization in Ethiopia, Kenya, Rwanda, Nigeria, and Ghana (Potapov *et al*., 2022).

The study area is already experiencing shocks from climate change and suffering from food insecurity (Mulugeta *et al*., 2018; Tofu *et al*., 2023). The changes in LULC could exacerbate these problems by reducing the availability of natural resources and increasing the vulnerability of the local population unless sustainable land use practices that balance economic development with environmental conservation are implemented.

The results of our analysis are consistent with the findings of the previous works (Entahabu *et al*., 2023; Woldemariam *et al*., 2022; Wudineh, 2023) which concluded that agricultural land and developed areas are expanding, whereas forest land, water bodies, and shrub land are shrinking. Furthermore, with the exception of the claim on an increase in water bodies linked to the growth of Lake Abaya's surface area, the results are consistent with the findings of the study carried out in the Gidabo River Basin, Ethiopia (Girma *et al*., 2022). Toma *et al*. (2023) also found that cultivated land, built-up area, and bare land expanded while shrub land and forest shrank annually between 1990 and 2020 in the Ajora-Woybo Watershed, Southern Ethiopia.

LULC change prediction

The findings of the predicted LULC changes showed a similar pattern to the historical LULC changes but with a slower rate. The future LULC change could have significant implications for the environment and the people living in the area. The decrease in waterbodies, forests, and shrubs could lead to a loss of biodiversity and ecosystem services, such as water regulation and carbon sequestration. The increase in development and agriculture could lead to habitat fragmentation, soil degradation, and increased greenhouse gas emissions. Promoting sustainable agricultural expansion policy and implementing natural resource management practices like soil and water conservation, re-afforestation, and afforestation of degraded land can help curb water resource reduction and expand barren land, thereby reducing the effects of agricultural land increase.

These results correspond to the works of Beshir *et al*. (2023) who simulated the LULC changes for 2037 and 2052 in the Upper WSRB. They discovered that the largest increases (23.80%) and decreases (7.84%) were in the areas of settlement and water bodies, respectively.

Conclusions and Recommendations

This study shows that during the past 40 years, the northeast WSRB has seen significant LULC alteration, mostly due to rapid urbanization and agricultural expansion. Significant increases in built-up, agricultural, and barren lands coincided with notable decreases in water bodies, forests, and shrub lands between 1985 and 2022, suggesting ongoing stress on natural ecosystems. These trends are predicted to continue through 2062, according to future simulations under the business-as-usual scenario, while the rate of change is anticipated to decline as the availability of highly appropriate land for conversion becomes scarcer. The successful implementation of the CA-Markov model and the Support Vector Machine (SVM) classifier validates its efficacy for both future land change prediction in the basin and historical LULC mapping. Overall, the results show that ongoing conversion of natural landscapes will progressively diminish ecosystem services, biodiversity, and water resources in the absence of effective intervention, endangering the basin's long-term environmental viability.

Strengthening integrated land management policies that strike a balance between urbanization, agricultural growth, and ecosystem preservation should be the top goal in order to promote sustainable land use in the northeast of the Wabi-Shebelle River Basin. The surviving forests, shrub lands, and bodies of water should be the main focus of conservation and restoration efforts, especially in the upper portion of the basin where natural ecosystems are still mostly intact. In order to direct future development toward appropriate locations and prevent further incursion into environmentally sensitive landscapes, land use planning should take the anticipated LULC changes into account. In order to facilitate prompt policy interventions and evidence-based decision-making, it is also necessary to institutionalize ongoing monitoring of land use patterns utilizing remote sensing and GIS technology. Lastly, lowering the strain on natural resources and guaranteeing the basin's long-term ecological resilience would require encouraging sustainable farming methods and involving nearby people in conservation efforts.

Declarations

Competing interests

The authors have no competing interests to declare that are relevant to the content of this article

Funding

The study was funded by Ministry of Education of Ethiopia and Haramaya University.

Data Availability Statement

The datasets generated during and/or analyzed during the current study are available from the corresponding author on reasonable request.

Author contributions

All the authors contributed to the conceptualization and design of the study. The corresponding author, Birhanu Legesse Wakjira, acquired and analyzed the data and wrote the manuscript. The other authors, Asfaw Kebede Kassa, Awdenegest Moges, and Olkeba Tolessa Leta, critically revised and strengthened the overall manuscript.

Acknowledgments

I would like to express gratitude to Ethiopian ministry of Education and Haramaya University for funding this research work. The majority of the materials and information utilized were gathered from the Ministry of Water and Energy and the National Meteorological Agency of Ethiopia and are gratefully acknowledged for granting access to the data.

References

Assede, E. S. P., Orou, H., Biaou, S. S. H., Geldenhuys, C. J., Ahononga, F. C. & Chirwa, P. W. (2023). Understanding Drivers of Land Use and Land Cover Change in Africa: A Review. *Current Landscape Ecology Reports*, 8(2), 62–72. https://doi.org/10.1007/s40823-023-00087-w

Awass, A. A. (2009). *Hydrological Drought Analysis-occurrence, severity, risks: the* *case of Wabi-Shebele River Basin, Ethiopia*. MSc. Thesis, University Siegen, Germany.

Balha, A., Singh, A., Pandey, S., Kumar, R., Mallick, J. & Singh, C. K. (2023). Assessing the Impact of Land-Use Dynamics to Predict the Changes in Hydrological Variables Using Effective Impervious Area (EIA). *Water Resources Management*, 37(10), 3999–4014. https://doi.org/10.1007/s11269-023-03536-7

Basheer, S., Wang, X., Farooque, A. A., Nawaz, R. A., Liu, K., Adekanmbi, T. & Liu, S. (2022). Comparison of Land Use Land Cover Classifiers Using Different Satellite Imagery and Machine Learning Techniques. *Remote Sensing*, 14(19). https://doi.org/10.3390/rs14194978

Bekele, T. (2019). Effect of Land Use and Land Cover Changes on Soil Erosion in Ethiopia. *International Journal of Agricultural Science and Food Technology*, 026–034. https://doi.org/10.17352/2455-815x.000038

Bell, E. J. (1974). Markov Analysis of Land Use Change-An Application of Stochastic Processes to Remotely Sensed Data. *Socio-Economic Planning Sciences*, 8(6), 311–316.

Beshir, S., Moges, A. & Dananto, M. (2023). Trend analysis, past dynamics and future prediction of land use and land cover change in upper Wabe-Shebele river basin. *Heliyon*, 9(9). https://doi.org/10.1016/j.heliyon.2023.e19128

Congalton, R. G. & Green, K. (2019). *Assessing the Accuracy of Remotely Sensed Data: Principles and Practices*. 3rd edition. CRC Press, Taylor & Francis Group, LLC. http://www.taylorandfrancis.com

Congedo, L. (2021). Semi-Automatic Classification Plugin: A Python tool for the download and processing of remote sensing images in QGIS. *Journal of Open Source Software*, 6(64), 3172. https://doi.org/10.21105/joss.03172

Cumani, R. & Latham, J. (2015). *FAO Land Cover Mapping methodology, tools and standards & GLC–SHARE database*. FAO meeting document, Rome, Italy.

Debnath, M., Islam, N., Gayen, S. K., Roy, P. B., Sarkar, B. & Ray, S. (2023). Prediction of spatio-temporal (2030 and 2050) land-use and land-cover changes in Koch Bihar urban agglomeration (West Bengal), India, using artificial neural network-based Markov chain model. *Modeling Earth Systems and Environment*, 2023, https://doi.org/10.1007/s40808-023-01713-6

Demissie, F., Yeshitila, K., Kindu, M. & Schneider, T. (2017). Land use/Land cover changes and their causes in Libokemkem District of South Gonder, Ethiopia. *Remote Sensing Applications: Society and Environment*, 8, 224–230. https://doi.org/10.1016/j.rsase.2017.10.001

Eastman, J. R. (2020). TerrSet Geospatial Monitoring and Modeling System, Tutorial Version 2020.v.19.0.0. *Angewandte Chemie International Edition*, 6(11), 449.

Entahabu, H. H., Minale, A. S. & Birhane, E. (2023). Modeling and Predicting Land Use/Land Cover Change Using the Land Change Modeler in the Suluh River Basin, Northern Highlands of Ethiopia. *Sustainability*, 15(10). https://doi.org/10.3390/su15108202

ESS, (Ethiopian Statistical Service) (2023). *Population Size by Sex, Region, Zone and Wereda*. July 2023. http://www.statsethiopia.gov.et/wp-content/uploads/2023/08/Population-of-Zones-and-Weredas-Projected-as-of-July-2023.pdf

FAO (Food and Agricultural Organization) (2016). *Map Accuracy Assessment and Area Estimation Map Accuracy Assessment and Area Estimation: A Practical Guide (46).* Rome, Italy, www.fao.org/publications.

Gebresellase, S. H., Wu, Z., Xu, H. & Muhammad, W. I. (2023). Scenario-Based LULC Dynamics Projection Using the CA–Markov Model on Upper Awash Basin (UAB), Ethiopia. *Sustainability*, 15(2), 1683. https://doi.org/10.3390/su15021683

Girma, R., Fürst, C. & Moges, A. (2022). Land use land cover change modeling by integrating artificial neural network with cellular Automata-Markov chain model in Gidabo river basin, main Ethiopian rift. *Environmental Challenges*, 6. https://doi.org/10.1016/j.envc.2021.100419

Goward, S., Arvidson, T., Williams, D., Faundeen, J., Irons, J. & Franks, S. (2006). Historical Record of Landsat Global Coverage: Mission Operations, NSLRSDA, and International Cooperator Stations. *Photogrammetric Engineering & Remote Sensing*, 72(10), 1155–1169. https://doi.org/https://doi.org/10.14358/PERS.72.10.1155.

Grover, H. D. & Musick, H. B. (1990). Shrubland encroachment in southern New Mexico, U.S.A.: An analysis of desertification processes in the American southwest. *Climatic Change*, 17(2–3), 305–330. https://doi.org/10.1007/BF00138373

Hailu, S. E. (2024). *Spatiotemporal Analysis of Land Use/Land Cover Change, and Their Implication on Climate Variability: The Case of Gobele Watershed of Wabi Shebelle Basin, Eastern Ethiopia*. MSc. Thesis, Haramaya University, Ethiopia.

Horamo, Y., Ayele, F. & Atiso, H. (2021). Land use and Land Cover Change Analysis, Causes and Effects on Agricultural Productivity, Case of Anlemo District in Hadiya zone, Ethiopia. *Himalayan Journal of Social Sciences and Humanities*, 16(1). https://doi.org/10.51220/hjssh.v16i1.2

Jansen, L. J. M. & Gregorio, A. Di. (2000). *Land Cover Classification System (LCCS): Classification Concepts and User Manual*. FAO, Rome, Italy.

Jozdani, S. E., Johnson, B. A. & Chen, D. (2019). Comparing deep neural networks, ensemble classifiers, and support vector machine algorithms for object-based urban land use/land cover classification. *Remote Sensing*, 11(14). https://doi.org/10.3390/rs11141713

Kebede, T. (2015). *Characterizing the Groundwater Potetial of Wabi-Shebelle River Basin*. MSc. Thesis, Addis Ababa University, Ethiopia.

Kutter, A., Nachtergaele, F. O. & Verheye, W. H. (2016). The new FAO approach to land use planning and management, and its application in Sierra Leone. *ITC Journal*, 3(4), 278-283. https://doi.org/https://www.researchgate.net/publication/290975923

Liang, X., Guan, Q., Clarke, K. C., Liu, S., Wang, B. & Yao, Y. (2021). Understanding the drivers of sustainable land expansion using a patch-generating land use simulation (PLUS) model: A case study in Wuhan, China. C*omputers, Environment and Urban Systems*, 85, 101569. https://doi.org/10.1016/j.compenvurbsys.2020.101569

Mulugeta, M., Tiruneh, G. & Alemu, Z. A. (2018). Magnitude and associated factors of household food insecurity in Fedis Woreda East Hararghe zone, Oromia region, Ethiopia. *Agriculture and Food Security*, 7(1), 1–8. https://doi.org/10.1186/s40066-017-0140-6

Munthali, M. G., Mustak, S., Adeola, A., Botai, J., Singh, S. K. & Davis, N. (2020). Modelling land use and land cover dynamics of Dedza district of Malawi using hybrid Cellular Automata and Markov model. Remote Sensing Applications: *Society and Environment*, 17. https://doi.org/10.1016/j.rsase.2019.100276

NWRC (National Water Resource Commission) (1973). *Soil Survey of the Wabi Shebelle Basin.* Addis Ababa, Ethiopia.

Olofsson, P., Foody, G. M., Herold, M., Stehman, S. V, Woodcock, C. E. & Wulder, M. A. (2014). Good practices for estimating area and assessing accuracy of land change. *Remote Sensing of Environment*, 148, 42–57. https://doi.org/10.1016/j.rse.2014.02.015

Pijanowski, B. C., Brown, D. G., Shellito, B. A. & Manik, G. A. (2002). Using neural networks and GIS to forecast land use changes: a Land Transformation Model. *Computers, Environment and Urban Systems*, 26(6), 553–575. https://doi.org/10.1016/S0198-9715(01)00015-1

Potapov, P., Hansen, M. C., Pickens, A., Hernandez-Serna, A., Tyukavina, A., Turubanova, S., Zalles, V., Li, X., Khan, A., Stolle, F., Harris, N., Song, X.-P., Baggett, A., Kommareddy, I. & Kommareddy, A. (2022). The Global 2000-2020 Land Cover and Land Use Change Dataset Derived from the Landsat Archive: First Results. *Frontiers in Remote Sensing*, 3. https://doi.org/10.3389/frsen.2022.856903

Puyravaud, J. P. (2003). Standardizing the calculation of the annual rate of deforestation. *Forest Ecology and Management*, 177(1–3), 593–596. https://doi.org/10.1016/S0378-1127(02)00335-3

Regasa, M. S., Nones, M. & Adeba, D. (2021). A review on land use and land cover change in ethiopian basins. *Land*, 10(6). https://doi.org/10.3390/land10060585

Roy, P. S., Ramachandran, R. M., Paul, O., Thakur, P. K., Ravan, S., Behera, M. D., Sarangi, C. & Kanawade, V. P. (2022). Anthropogenic Land Use and Land Cover Changes—A Review on Its Environmental Consequences and Climate Change. In *Journal of the Indian Society of Remote Sensing*, 50 (8), 1615–1640). https://doi.org/10.1007/s12524-022-01569-w

Rwanga, S. S. & Ndambuki, J. M. (2017). Accuracy Assessment of Land Use/Land Cover Classification Using Remote Sensing and GIS. *International Journal of Geosciences*, 8, 611–622. https://doi.org/https://doi.org/10.4236/ijg.2017.84033

Saigal, P. (2021). Introduction to Support Vector Machines. In P. Saigal (Ed.), *Support Vector Machines: Evolution and Application* (pp. 1–10). Nova Science Publishers, Inc.

Tofu, D. A., Mekuria, M. M. & Ogato, G. S. (2023). Climatic extremes' resilient livelihoods of rural households in the Eastern Ethiopia. *Agriculture and Food Security*, 12(1). https://doi.org/10.1186/s40066-023-00446-0

Toma, M. B., Belete, M. D. & Ulsido, M. D. (2023). Historical and future dynamics of land use land cover and its drivers in Ajora-Woybo watershed, Omo-Gibe basin, Ethiopia. *Natural Resource Modeling*, 36(1). https://doi.org/10.1111/nrm.12353

Toni, A. T., Malcherek, A. & Kassa, A. K. (2022). Agroclimatic Zone-Based Analysis of Rainfall Variability and Trends in the Wabi Shebele River Basin, Ethiopia. *Water*, 14(22). https://doi.org/10.3390/w14223699

van Vliet, J., Bregt, A. K. & Hagen-Zanker, A. (2011). Revisiting Kappa to account for change in the accuracy assessment of land-use change models. *Ecological Modelling*, 222(8), 1367–1375. https://doi.org/https://doi.org/10.1016/j.ecolmodel.2011.01.017

Verburg, P. H., Soepboer, W., Veldkamp, A., Limpiada, R., Espaldon, V. & Mastura, S. S. A. (2002). Modeling the spatial dynamics of regional land use: The CLUE-S model. *Environmental Management*, 30(3), 391–405. https://doi.org/10.1007/s00267-002-2630-x

Viera, A. J. & Garrett, J. M. (2005). Understanding Interobserver Agreement: The Kappa Statistic. *Research Series*, 35(5), 360–363.

Wang, Y., Zhao, X., Zuo, L., Zhang, Z., Wang, X., Yi, L., Liu, F. & Xu, J. (2020). Spatial differentiation of land use and landscape pattern changes in the Beijing-Tianjin-Hebei area. *Sustainability*, 12(7). https://doi.org/10.3390/su12073040

White, R. & Engelen, G. (1993). Cellular Automata and Fractal Urban Form: A Cellular Modelling Approach to the Evolution of Urban Land-Use Patterns. *Environment and Planning A*, 25(8), 1175–1199.

Wolde, B., Moges, A. & Grima, R. (2023). Assessment of the combined effects of land use/land cover and climate change on soil erosion in the Sile watershed, Ethiopian Rift Valley Lakes Basin. *Cogent Food and Agricultur*e, 9(2). https://doi.org/10.1080/23311932.2023.2273630.

Woldemariam, G. W. & Harka, A. E. (2020). Effect of land use and land cover change on soil erosion in erer sub-basin, Northeast Wabi-Shebelle Basin, Ethiopia. *Land*, 9(4), 1–25. https://doi.org/10.3390/land9040111

Woldemariam, G. W., Tibebe, D., Mengesha, T. E. & Gelete, T. B. (2022). Machine-learning algorithms for land use dynamics in Lake Haramaya Watershed, Ethiopia. *Modeling Earth Systems and Environment*, 8(3), 3719–3736. https://doi.org/10.1007/s40808-021-01296-0

Wudineh, F. A. (2023). Land-use and land-cover change and its impact on flood hazard occurrence in Wabi-Shebele River

Basin of Ethiopia. *Hydrology Research*, 54(6), 756–769. https://doi.org/10.2166/nh.2023.121

Yohannes, H., Mohammed, A. & Elias, E. (2017). Land Use/Land Cover Dynamics and Its Impact on Biodiversity Resources in the Abijata Shalla National Park, Central Rift Valley Lakes Region, Ethiopia. *Environmental Science: An Indian Journal*, 13(5). www.tsijournals.com

Zhang, Y., Woodcock, C. E., Arévalo, P., Olofsson, P., Tang, X., Stanimirova, R., Bullock, E., Tarrio, K. R., Zhu, Z. & Friedl, M. A. (2022). A Global Analysis of the Spatial and Temporal Variability of Usable Landsat Observations at the Pixel Scale. *Frontiers in Remote Sensing*, 3. https://doi.org/10.3389/frsen.2022.894618

Zhao, Q., Wen, Z., Chen, S., Ding, S. & Zhang, M. (2020). Quantifying land use/land cover and landscape pattern changes and impacts on ecosystem services. *International Journal of Environmental Research and Public Health*, 17(1). https://doi.org/10.3390/ijerph17010126.